Progressive changes in T_1, T_2 and left-ventricular histo-architecture in the fixed and embedded rat heart

Patrick W. Hales[a,*], **Rebecca A.B. Burton**[b], **Christian Bollensdorff**[b], **Fleur Mason**[b], **Martin Bishop**[c], **David Gavaghan**[c], **Peter Kohl**[b], and **Jürgen E. Schneider**[a]

[a]Department of Cardiovascular Medicine, University of Oxford, Oxford, UK

[b]Department of Physiology, Anatomy and Genetics, University of Oxford, Oxford, UK

[c]Computing Laboratory, University of Oxford, Oxford, UK

Abstract

Chemical tissue fixation, followed by embedding in either agarose or Fomblin, is common practice in time-intensive MRI studies of *ex vivo* biological samples, and is required to prevent tissue autolysis and sample motion. However, the combined effect of fixation and sample embedding may alter tissue structure and MRI properties. We investigated the progressive changes in T_1 and T_2 relaxation times, and the arrangement of locally prevailing cardiomyocyte orientation determined using diffusion tensor imaging, in embedded *ex vivo* rat hearts fixed using Karnovsky's solution (glutaraldehyde–formaldehyde mix). Three embedding media were investigated: (i) standard agarose ($n = 3$ hearts); (ii) Fomblin ($n = 4$ hearts); and (iii) iso-osmotic agarose ($n = 3$ hearts); in the latter, the osmolarity of the fixative and embedding medium was adjusted to 300 mOsm to match more closely that of native tissue. The T_1 relaxation time in the myocardium showed a pronounced decrease over a 48-h period following embedding in Fomblin ($-11.3 \pm 6.2\%$; mean $\pm$ standard deviation), but was stable in standard agarose- and iso-osmotic agarose-embedded hearts. The mean myocardial T_2 relaxation time increased in all embedded hearts: by $35.1 \pm 14.7\%$ with standard agarose embedding, $13.1 \pm 5.6\%$ with Fomblin and $13.3 \pm 1.4\%$ with iso-osmotic agarose. Deviation in the orientation of the primary eigenvector of the diffusion tensor occurred in all hearts (mean angular changes of 6.6°, 3.2° and 1.9° per voxel after 48 h in agarose-, Fomblin- and iso-osmotic agarose-embedded hearts, respectively), indicative of progressive structural changes in myocardial histo-architecture, in spite of previous exposure to fast-acting tissue fixation. Our results suggest that progressive structural changes occur in chemically fixed myocardium, and that the extent of these changes is modulated by the embedding medium, and by osmotic gradients between the fixative in the tissue and the surrounding medium.

Keywords

diffusion tensor imaging; myocardium; structure; tissue fixation; Karnovsky's fixative; cone of uncertainty; precision; myofibre

---

*Correspondence to: P. W. Hales, Radiology and Physics (Biophysics), UCL Institute of Child Health, 30 Guilford Street, London, WC1N 1EH, UK. phales@ich.ucl.ac.uk.

INTRODUCTION

Myocardial histo-architecture is known to have a profound impact on the physiological properties of the heart, influencing both mechanical (1) and electrical (2) behaviour. Over recent years, diffusion tensor imaging (DTI) has emerged as a powerful tool for the nondestructive determination of the histo-architectural properties of the heart (3–6). Using this method, the voxel-wise diffusion tensor can be decomposed into its eigenvectors to provide information regarding the locally prevailing orientation of myocytes, whose longitudinal direction is usually (if histo-anatomically incorrectly) referred to as 'fibre orientation'. The eigenvalues of the diffusion tensor can be used to determine scalar properties, such as the apparent diffusion coefficient (ADC) and fractional anisotropy (FA), which describe the local magnitude and spatial distribution of water diffusibility, respectively. In addition to determining the 'myofibre architecture' in healthy left-ventricular myocardium (7–9), DTI has also been used to quantify the structural changes caused by pathologies such as ischaemia (10–12).

Currently, the majority of cardiac DTI studies are performed on *ex vivo* hearts, particularly when high-resolution three-dimensional data are required. This is primarily because of the long scan times required to collect these datasets (8,13), as well as the susceptibility of the technique to motion and flow artefacts (14). In order to prevent autolysis in *ex vivo* samples during this period, tissue is generally fixed using either formaldehyde-based solutions, such as formalin, or a formaldehyde–glutaraldehyde mix, such as Karnovsky's fixative. Formaldehyde fixation facilitates rapid tissue penetration because of the small size of formaldehyde molecules, and initial binding to proteins generally occurs within 24 h (15). However, the formation of inter-protein methylene bridges required for complete tissue stabilisation proceeds much more slowly, and complete tissue fixation may require several weeks (16). Conversely, glutaraldehyde molecules react quickly to ensure rapid cross-linking of proteins, and can render tissue resistant to osmotic stress after 24 h of fixation (17). However, tissue penetration is 10 times slower than with formaldehyde (18). Karnovsky's solution [a mixture of glutaraldehyde and formaldehyde in cacodylate buffer (19)] is superior to either aldehyde fixative alone, as formaldehyde rapidly penetrates the tissue to swiftly 'pre-stabilise' proteins in a given configuration (important, in particular, for mechanically active tissues such as the heart), which are then permanently fixed by glutaraldehyde. Therefore, we chose to use this fixative in the present study of left-ventricular histo-anatomy.

Following fixation, *ex vivo* samples can be embedded in aqueous gels, such as low-melting-temperature agarose (20–22) or gelatine (7), or in water-free substances, such as Fomblin (8,10,23). The later is a perfluoropolyether with a low dielectric effect, which is susceptibility matched to tissue and produces no MR signal, facilitating the segmentation of tissue from the surrounding embedding medium during post-processing. However, gel embedding has the advantage that motion artefacts, for instance those caused by gravitational forces or by vibrations during rapid gradient switching for high-resolution DTI scans, will be minimised, as the sample is 'fixed in place' more firmly within the test tube by a more viscous embedding medium. This is not the case with liquid Fomblin embedding, in which the myocardial tissue samples can float if not properly filled and restrained, and

therefore more complex mounting approaches may be required to prevent sample motion during DTI.

The action of aldehyde fixation on the cross-linking of proteins throughout the intra- and extracellular spaces of tissues alters the local chemical environment, which, in turn, will alter MRI contrast mechanisms (24). This may lead to erroneous extrapolation from *ex vivo* MRI data to the *in vivo* setting. Several groups have investigated fixation-induced changes in parameters such as the T_1 and T_2 relaxation times and water diffusion in non-cardiac tissues, such as the human brain (25,26), mouse brain (27), rat nervous tissue (24,28), human and pig spinal cord (29), bovine nasal cartilage (30) and model biological tissues comprising erythrocyte ghosts suspended in buffer and agarose (31). The progressive effect of tissue fixation, once the sample is removed from the fixative and placed in a surrounding embedding medium, has not yet been investigated, however, and data on fixation effects on cardiac tissue are missing. Here, we examine the progressive effect of tissue fixation and embedding on MR parameters and cardiac histo-anatomy using excised rat hearts. As a high-resolution (~ 100 μm) DTI scan can take 48 h or more to complete [8,13], we aimed to assess the stability of the magnetisation relaxation and DTI parameters in *ex vivo* embedded rat myocardium over a similar time period. The dependence of these parameters on the type of embedding medium used (either low-melting-temperature agarose or Fomblin) and the osmolarity of the fixative was also investigated.

METHODS

Sample preparation

All investigations conform to the UK Home Office guidance on the Operation of Animals (Scientific Procedures) Act of 1986. Hearts were isolated from female Sprague Dawley rats [246 ± 19 g, mean ± standard deviation (SD)] after cervical dislocation, and swiftly (< 90 s) connected via the aorta to a constant-flow (5–6 mL/min) Langendorff perfusion system (32). An incision in the pulmonary artery was made to avoid the build-up of fluid reaching the right heart via the coronary circulation. The tissue was initially washed (2 min) with heparin-containing 'normal Tyrode' (NT) solution [containing 140 m$_M$ NaCl, 5.4 m$_M$ KCl, 1 m$_M$ MgCl$_2$, 1.8 m$_M$ CaCl$_2$, 11 m$_M$ glucose, 5 m$_M$ *N*-2-hydroxyethylpiperazine-*N′*-2-ethanesulphonic acid (HEPES) and 5 IU/mL heparin, oxygenated] before cardioplegic arrest was induced by perfusion with high-potassium solution (HiK$^+$; 20 m$_M$ KCl, 125 m$_M$ NaCl, 1 m$_M$ MgCl$_2$, 1.8 m$_M$ CaCl$_2$, 11 m$_M$ glucose, 5 m$_M$ HEPES, oxygenated). Immediately after cardiac arrest, tissue was fixed by coronary perfusion with 20 mL of the fast-acting Karnovsky's fixative [2% formaldehyde and 2.5% glutaraldehyde mix in sodium cacodylate buffer (19); see Table 1]. During the whole procedure, hearts were positioned in a fluid-filled glass container to keep their cavities free from bubbles. Fixed hearts were stored in Karnovsky's fixative for 24 h prior to embedding [for details, see ref. (13)].

For embedding, hearts were repeatedly rinsed in sodium cacodylate buffer (60 min at 4°C), and then processed depending on protocols (i)–(iii): (i) For the standard agarose preparation, hearts were stabilised in a 28-mm-diameter NMR tube using low-melting-point 2% agar (NuSieve GTG Agarose 50080, Lonza, Slough, Berkshire, UK). Cacodylate buffer was left inside the cavities to prevent the ventricle walls from collapsing. (ii) For the Fomblin

preparation, hearts were stabilised using an in-house-designed cradle inside the NMR tube, which was then filled with Fomblin (Series LC08, Performance Fluids, Nelson, Lancashire, UK). Fomblin was also syringed into the ventricular cavities to replace the sodium cacodylate buffer. Intra and extra-cardiac cavities were continuous with each other, preventing the build-up of transmural pressure gradients. (iii) For the iso-osmotic agarose preparation, the osmolarity of all solutions (including Karnovsky's, cacodylate buffer and agar) was maintained at 300 ± 5 mOsm. The agar for this preparation was prepared by dissolving 2 g of low-melting-point agar in 100 mL of 300 mOsm cacodylate buffer [instead of distilled water as used in (i)]. Cardiac cavities were filled with buffer, and the preparation was embedded in the NMR tube. The hearts prepared using the methods described above are referred to as: (i) standard agarose; (ii) Fomblin; and (iii) iso-osmotic. In total, 10 hearts were embedded [$n = 3$ for preparation (i), $n = 4$ for (ii) and $n = 3$ for (iii)], and scanned in a horizontal position within the magnet.

Image acquisition

Hearts were imaged using a Varian 9.4-T (400 MHz) MR system (Varian Inc., Palo Alto, CA, USA), comprising a horizontal magnet (bore size, 210 mm), a VNMRS Direct Drive console and shielded gradient system (1 T/m; rise time, 130 μs). A birdcage coil with an inner diameter of 28 mm (Rapid Biomedical, Rimpar, Germany) was used to transmit–receive the NMR signals. Data acquisition was initiated as soon as possible after sample embedding (3.7 ± 0.2 h, all samples mean $\pm$ SD), and continued over a period of 48 h. All experiments were conducted at the ambient temperature inside the magnet (19.1 ± 0.8°C, all samples mean $\pm$ SD), and the temperature throughout the testing of an individual sample was stable to within ± 0.5°C.

T_1 and T_2 data acquisition

T_1 measurements were made using a snapshot FLASH (fast low-angle shot) two-dimensional multi-slice pulse sequence (33), with segmented k-space acquisition (64 k-space lines per segment), and a final data matrix size of 128×128 over a 26×26 mm^2 field of view (FOV). Five axial slices (thickness, 1 mm) were equally spaced from the apex to the base of the heart, and data were acquired at 10 points during each inversion recovery (TE/TR = 1.37/2.84 ms; TR/segment = 187.0 ms). The delay between inversion pulses was greater than $5 \times T_1$. Ten averages were acquired for each image, resulting in a total scan duration of 10 min.

T_2 was measured with a multi-spin-echo two-dimensional pulse sequence (same slice and data matrix parameters as used for T_1 data acquisition, but sampling four averages). Sixteen echoes were collected per excitation, with TR = 4s and   TE = 5.2 ms. The total scan duration was 34 min.

DTI data acquisition

Three-dimensional DTI data were obtained using a fast spin-echo diffusion-weighted pulse sequence. The FOV was $26 \times 26 \times 26$ mm, with a data matrix of $64 \times 64 \times 64$, resulting in an isotropic resolution of 406 μm. Eight echoes were acquired per excitation, with TR = 1 s. The central line of k space was collected during the third echo, resulting in an effective TE

(TE$_{eff}$) of 36.3 ms. Unipolar diffusion gradients were applied in six directions according to an optimised scheme based on the electrostatic repulsion principle (34), with a gradient strength of 30 G/cm, duration of 2.5 ms and separation of 15 ms. This resulted in a *b* value of 703 s/mm^2, accounting for all imaging gradients and cross-terms between imaging and diffusion gradients (35). The number of signal averages (NSA) acquired was three, and the scan duration was 3 h per acquisition.

In order to investigate the influence of resolution, diffusion gradient scheme and diffusion weighting (*b* value), two-dimensional DTI data were also acquired at each time point, using a fast spin-echo pulse sequence with eight echoes per excitation and the following acquisition parameters: TR = 2 s; TE$_{eff}$ = 25 ms (central line of *k* space was collected during the first echo); FOV, 26 × 26 mm; matrix size, 128 × 128; in-plane resolution, 203 μm; slice thickness, 1 mm; 21 contiguous slices covering the entire length of the heart. Unipolar diffusion gradients were applied in 15 directions (again using a scheme based on electrostatic repulsion), with a gradient strength of 30 G/cm, duration of 2.7 ms, separation of 20 ms and a *b* value of 1040s/mm^2.

All imaging protocols were repeated at 4.2-h intervals over a 48-h period, without removing the sample from the magnet. In order to additionally assess the long-term stability of the three embedding techniques, the above protocol was repeated for one heart from each group, 1 week after embedding. In addition, a single heart from the most stable group [iso-osmotic agarose, (iii)] was re-scanned 1 month later for the bootstrap analysis described below.

Data analysis

T_1 and T_2 values were calculated by applying a monoexponential fit to the image data. The signal-to-noise ratio (SNR) was measured in the myocardium at each time point, using the unweighted (*b* = 0) images in the DTI datasets. Diffusion tensors were calculated on a voxel-by-voxel basis via a weighted linear least-squares fitting method, using in-house software developed in IDL (ITT Corporation, Boulder, CO, USA). Tensors were then diagonalised to produce the sorted eigenvectors (ν_1, ν_2, ν_3) and eigenvalues (λ_1, λ_2, λ_3). From these, FA and ADC were calculated using:

$$\text{FA} = \frac{\sqrt{(\lambda_1 - \lambda_2)^2 + (\lambda_2 - \lambda_3)^2 + (\lambda_1 - \lambda_3)^2}}{\sqrt{\left[2\left(\lambda_1^2 + \lambda_2^2 + \lambda_3^2\right)\right]}} \quad (1)$$

$$\text{ADC} = \frac{(\lambda_1 + \lambda_2 + \lambda_3)}{3} \quad (2)$$

Changes in FA, ADC and ν_1 [the primary eigenvector, which is aligned to the locally prevailing cell orientation (5,6)] were measured on a voxel-by-voxel basis at each time point. Temporal deviations in ν_1 were determined by measuring the angle (θ) between the primary eigenvector at a given time point $\nu_1(t)$, and the primary eigenvector in the same voxel at the first time point $\nu_1(t_0)$, i.e.

$$\theta = \arccos \left[\left| \boldsymbol{v}_1(t) \cdot \boldsymbol{v}_1(t_0) \right| \right] \quad (3)$$

The orientation of voxel-wise primary eigenvectors was also expressed in terms of the helix angle a (36). The helix angle is the angle between the projection of the primary eigenvector onto the tangential plane (parallel to the epicardial surface) and the transverse (equatorial) plane of the heart. Myofibre orientation generally undergoes a smooth transition from a left-handed helical arrangement at the epicardium, to an equatorially circumferential arrangement in the mid-ventricular wall, to a right-handed helical arrangement in subendocardial tissue [e.g. refs. (4,37)]. The prevailing myofibre population in each DTI voxel in the myocardium was categorised into three types: left-handed helical fibre (LHF), $-60° < a < -30°$; circumferential fibre (CF), $-30° \quad a \quad 30°$; and right-handed helical fibre (RHF), $30° < a < 60°$ (38). Using multiple regions of interest spanning the septal, anterior, lateral and interior walls of the left ventricle, regional changes in the fraction of LHF, CF and RHF over time were quantified.

Cone of uncertainty (COU) measurements

In order to quantify the precision of the $\boldsymbol{v}_1$ measurement, and to examine how this varies with changes in SNR, we performed tests on an iso-osmotic agarose-embedded (iii) heart, 1 month after embedding. The heart was removed from the scanner in the interim period, but remained embedded in the NMR tube, and was stored at 4°C. First, we verified that the sample was stable in terms of $\boldsymbol{v}_1$ orientation (SD of 0.1° over 48 h). The three-dimensional DTI protocol described above was then carried out three times with NSA = 1, and repeated with an increasing number of averages to collect replicates of the three-dimensional DTI data over an SNR range of 140–370 (SNR was measured using the unweighted $b = 0$ image). The repeated DTI measurements were used to carry out a bootstrap analysis of the precision of the measurements of $\boldsymbol{v}_1$. The method used was similar to that described in ref. (39). Briefly, the replicates of the DTI experiments (at a fixed SNR) were used to create 100 bootstrap samples of a complete DTI dataset from the collective pool of data, by randomly selecting (with replacement) one measurement for each gradient direction including a $b = 0$ image [i.e. no diffusion weighting, see detail in ref. (39)]. The mean primary eigenvector of the 100 bootstrap samples (Ψ_1) was calculated in each voxel using the dyadic formalism described in ref. (40). The angular deviation between each of the bootstrap samples of $\boldsymbol{v}_1$ and Ψ_1 was calculated in each voxel, and the 95% percentile of these 100 values was taken as the 95% confidence interval (or COU of Ψ_1 for that voxel). The COU is equivalent to the precision in the measurement of $\boldsymbol{v}_1$ for a given level of SNR. This process was repeated over the range of SNR values, so that the variation in COU could be measured as a function of SNR.

Statistical analysis

Unless otherwise stated, scalar DTI parameters and T_1 and T_2 values are expressed as the mean value over all voxels within the myocardium, and all data are shown as the mean ± SD. All statistical analysis was performed using SPSS (SPSS, Chicago, IL, USA). The first and last points in the time series of the relaxation time and DTI parameter measurements

were compared using a two-tailed unpaired t-test. A value of $p < 0.05$ was considered to be statistically significant.

RESULTS

T_1 and T_2 relaxation times

Initial values of the mean T_1 and T_2 relaxation times in the myocardium, measured at the first time point (t_0), are given in Table 2. The standard agarose- (i) and Fomblin-embedded (ii) hearts started with similar T_1 values at t_0, but the iso-osmotically embedded (iii) hearts had initial T_1 values that were approximately 50% higher [$p < 0.01$ cf. (i) and (ii)]. The initial T_2 relaxation time was also highest in the iso-osmotically embedded hearts, but only significantly so when compared with the Fomblin group [mean T_2 in (iii) was 92% higher than the mean T_2 in (ii), $p < 0.05$].

The time series of the mean myocardial T_1 and T_2 values for each preparation (normalised with respect to the first time point t_0) are shown in Fig. 1. Mean myocardial T_1 values decreased over time in the Fomblin-embedded (ii) hearts, showing a significant ($- 11.3 \pm 6.2\%$) reduction by the final time point t_f, 48 h after embedding ($p = 0.04$). However, in the standard (i) and iso-osmotic (iii) agarose-embedded hearts, stable myocardial T_1 values were observed ($p > 0.05$). T_2 values in the myocardium increased rapidly over time in standard agarose-embedded hearts (increase of $+ 35.1 \pm 14.7\%$ at t_f compared with t_0, $p = 0.03$), whereas both Fomblin- and iso-osmotically embedded hearts showed a gradual increase in myocardial T_2 (ii: $+ 13.1 \pm 5.6\%$, $p = 0.02$; iii: $+ 13.3 \pm 1.4\%$, $p = 0.04$).

DTI

The initial values of the mean FA and ADC in the myocardium of each heart are given in Table 2. Mean values of FA and ADC were not statistically significantly different between any of the groups. In addition, the time course of mean myocardial FA and ADC values showed no statistically significant change over 48 h ($p > 0.05$).

The mean value of θ [the mean voxel-wise angular deviation of v_1 compared with $v_1(t_0)$] as a function of time is shown for all preparations in Fig. 2. Each value is normalised to the value at the first time point following the start of the experiment ($t_1 = 4.2$ h) in order to illustrate the change in the deviation of v_1 over time. A clear increase is seen in the mean value of θ over time in all preparations. However, in the standard agarose-embedded (i) hearts, the increase in θ is more pronounced. The mean value of θ at t_1 was $4.0 \pm 0.3°$ in this group and, by t_f, this had increased to $10.5 \pm 1.4°$ (a $6.5°$ increase in the mean angular deviation of v_1 over 44 hours). In the Fomblin (ii) and iso-osmotic agarose (iii) groups, the increase in θ was considerably lower ($3.2°$ and $1.9°$, respectively see Table 2). A very similar pattern was observed in the two-dimensional multi-slice DTI data, where the observed mean increase in θ at t_f was $5.2°$ after 48 h in the standard agarose-embedded (i) hearts, whereas, in the Fomblin- (ii) and iso-osmotic agarose-embedded (iii) hearts, it was $2.7°$ and $1.3°$, respectively (data not shown).

Effect of SNR on COU and θ(t)

The measured COU around ν_1 decreased from 5.9° at SNR = 140 to 2.8° at SNR = 370, and followed the following relation:

$$\text{COU} \propto \text{SNR}^{-0.7} \quad (4)$$

with $R^2 = 0.97$. The mean SNR at t_0 was 324 ± 26 in standard agarose- (i), 188 ± 30 in Fomblin- (ii) and 218 ± 94 in iso-osmotic agarose-embedded (iii) hearts. As SNR changed throughout the course of the experiments in all hearts (Table 3), because of the continuous changes in the T_1 and T_2 relaxation times, the resultant change in precision in the measurement of ν_1 had to be accounted for. As SNR was measured at each time point (using the $b = 0$ image for each DTI dataset), and the relationship between SNR and COU had also been measured, we were able to plot the expected level of precision in the measurement of ν_1 at each time point in conjunction with θ(t). An example of this for standard agarose-embedded hearts (i) is shown in Fig. 3. The mean value of θ at the first time point (mean change in orientation of ν_1 at $t_1 = 4$ h, compared with t_0) already exceeds the variation expected as a result of the precision in the measurement of ν_1. Between t_1 and t_f (48 h), the value of θ increased steadily, by 6.6°, whereas the change in COU was only 0.3°. In Table 3, the mean changes in θ, COU (precision) and SNR at t_f for each group are shown. In all preparations, the changes observed in the mean value of θ are at least six times greater than the change in the precision.

Sample stability 1 week after embedding

Only minor changes in T_1, T_2 and θ were observed in all samples 1 week after embedding: the overall mean changes in T_1 and T_2 were $2.2 \pm 2.1\%$ and $1.7 \pm 1.4\%$, respectively, over a 48-h period (mean $\pm$ SD of the three hearts tested, one from each group; $t_f = 48$ h compared with t_0). Most importantly, the value of θ remained effectively constant, with variations in the mean value of just $0.3 \pm 0.1°$ between t_0 and t_f.

Helix angles

The mean change at t_f in the fractions of LHF, CF and RHF in the four aspects of the left-ventricular wall (septum, anterior, lateral, interior) are shown for all hearts in Fig. 4. The only regional change that is statistically significant for all hearts is the decrease in the fraction of CF in the septal wall (mean decrease of $- 3.1\%$ for all hearts, $p = 0.03$).

DISCUSSION

T_1 and T_2 relaxation

It has been shown previously in non-cardiac tissue that the action of aldehyde-based fixatives on *ex vivo* samples decreases the T_1 and T_2 relaxation times from their prefixation values (24–26). It has also been reported that washing non-cardiac tissue samples in buffer after fixation can reverse the initial decrease in T_2 values caused by fixation (31,41). This can be explained by the fact that washing removes free fixative from the interstitial spaces in the tissue (41). Our results show that T_2 values continue to increase in all embedded Karnovsky's fixed hearts (all of which were washed with cacodylate buffer following

fixation) up to 48 h post-embedding. The continuous increase in T_2 could be indicative of a reduction of free fixative in the tissue, caused by continued reactions between the free fixative and tissue and the loss of fixative from the tissue as a result of osmolarity gradients between fixed tissue and embedding medium. The increase in T_2 is much greater in standard agarose-embedded hearts (i), which is the only embedding approach used that is associated with a large osmotic gradient between interstitial fluid and an embedding medium that contains water (i.e. agarose). This may result in an influx of water from the embedding medium into the myocardium, and subsequent 'dilution' of free fixative in the tissue. Both the influx of water (inherently resulting in higher T_2 values) and the dilution of unreacted fixative could contribute to an increase in myocardial T_2. This influx of water into the myocardium does not occur in Fomblin-embedded hearts because of the lack of water in the embedding medium. It is also unlikely to occur in the iso-osmotically embedded hearts because of the lack of osmotic gradients. Accordingly, the change in T_2 values in these two embedding protocols follows a similar trend and reaches less pronounced peak levels, compared with standard agarose embedding. The remaining slow increase in T_2 relaxation times observed in these hearts may be a result of a gradual reaction of residual unreacted fixative with the myocardium, which would slowly decrease the remaining bulk fixative in the interstitial spaces in the tissue.

It has also been shown that changes in T_1 values, caused by aldehyde fixation, are not a result of the presence of bulk fixative in the tissue *per se*, but of continued chemical reactions between fixative and tissue; therefore, washing samples after fixation does not reverse the reduction in T_1 relaxation times caused by the fixative (24). All samples in this study were perfusion fixed via the coronary vasculature, ensuring optimal and swift delivery of the fixative to all cells of the heart [each myocyte is surrounded by four to five capillaries in the myocardium of healthy Sprague Dawley rats (42)], and this was followed by immersion fixation for 24 h before embedding. However, the continued decay in T_1 values observed in Fomblin-embedded hearts is indicative of progressive effects of the fixative on the myocardium, after the sample has been removed from the fixative. This could be a result of the continuous, slow action of the 'second-stage' formaldehyde fixation process, in which protein-bound formaldehyde molecules continue to react with free proteins, forming methylene cross-links (16). If this is the case, continuous action of the second-stage formaldehyde fixation process is much reduced in the agarose- (i) and iso-osmotic-embedded (iii) hearts, as T_1 is relatively stable in these samples. In the case of (i), the influx of water into the myocardium from the surrounding embedding medium may have interfered with progressive tissue–fixative interactions. In the case of (iii), the reduction in continued tissue–fixative interactions could be a consequence of the lower osmolarity Karnovsky's solution used in this preparation, which was approximately five times more dilute compared with the 'standard' approach. This would also explain why the initial myocardial T_1 values were much higher in the iso-osmotic hearts: T_1 shortening caused by tissue fixation is less pronounced when a dilute Karnovsky's solution is used.

DTI parameters

The fact that the angular deviation of the primary eigenvectors increases steadily over time in all hearts suggests that progressive structural changes in the myofibre orientation occur,

regardless of the type of embedding used. However, one must also consider the influence that changes in SNR, as a result of changes in the T_1 and T_2 relaxation time, may have on the measurements. The results shown in Table 3 confirm that any change in COU over 48 h would be very small in all hearts. In addition, the group that experienced the greatest change in SNR over the 48-h period was that using iso-osmotic embedding (iii; mean increase of 12.0%); this group showed the lowest mean change in θ (1.9°).

The fact that the time course of θ follows a similar pattern in the two-dimensional and three-dimensional DTI data suggests that the changes observed in ν_1 are reproducible when the diffusion gradient scheme, b value and spatial resolution are altered. Overall, this confirms that the change in θ over time primarily represents actual structural change, rather than an artefact of the measurement process.

Regional structural change

The decrease in the fraction of circumferentially oriented myofibres in the septal wall over time is an area that warrants further investigation. The ventricular cavities remained filled with buffer/Fomblin throughout the experiments, and so it is possible that the shift in fibre orientation is a result of internal stresses in the myocardium, caused by changes in water content, and possibly osmotic pressure in preparation (i).

Previous studies by our group have investigated the propagation of electrical activation within MR-derived computational three-dimensional finite element models of the ventricles [method described in refs. (13,43)]. We have shown that a mean angular change in the orientation of ν_1 of just 3° can result in a 10% change in electrical activation time in some regions of the myocardium, following an initial electric stimulus (Hales PW, Bishop M). In areas in which the proportion of CF has decreased, and the proportion of LHF has increased, modelled electrical propagation will be artificially faster in the apico-basal direction, because of a higher proportion of longitudinally oriented fibres, and will reduce the accuracy in the representation of the physiological behaviour of the heart, as it would have been seen *in vivo*.

Thus, during time-intensive MRI or DTI studies of *ex vivo* hearts, it is important to ensure that the MR and tissue water diffusion characteristics remain stable. Although tissue fixation and sample embedding are necessary, we have shown that the combined effect of the two processes may not prevent, or even increase, changes in MR properties representative of cardiac histo-anatomical structure over time. Preparation (i) (standard agarose embedding) showed the greatest increase in θ and T_2 over 48 h, and it is therefore the least favourable preparation method. Preparation (iii) (iso-osmotic embedding) showed the lowest absolute change in θ, and resulted in the most stable T_1 and T_2 values, making it the most stable sample embedding method investigated. Continuous structural change can be reduced by scanning tissue 1 week after fixation. However, this only offers an apparent solution to the problem, as the tissue, although more stable, will be less representative of its native state after this period of fixation. Further research is needed to characterise the detailed effects of fixation on myocardial histo-anatomy over time.

Acknowledgements

Abbreviations used

|	
ADC	apparent diffusion coefficient
CF	circumferential fibre
COU	cone of uncertainty
DTI	diffusion tensor imaging
FA	fractional anisotropy
FLASH	fast low-angle shot
FOV	field of view
HiK$^+$	high-potassium solution (modified Tyrode solution)
LHF	left-handed helical fibre
NSA	number of signal averages
NT	normal Tyrode
RHF	right-handed helical fibre
SD	standard deviation
SNR	signal-to-noise ratio

REFERENCES

1. Waldman LK, Nosan D, Villarreal F, Covell JW. Relation between transmural deformation and local myofiber direction in canine left ventricle. Circ. Res. 1988; 63:550–562. [PubMed: 3409487]

2. Kanai A, Salama G. Optical mapping reveals that repolarization spreads anisotropically and is guided by fiber orientation in guinea pig hearts. Circ. Res. 1995; 77:784–802. [PubMed: 7554126]

3. Holmes A, Scollan D, Winslow R. Direct histological validation of diffusion tensor MRI in formaldehyde-fixed myocardium. Magn. Reson. Med. 2000; 44:157–161. [PubMed: 10893534]

4. Jiang Y, Pandya K, Smithies O, Hsu E. Three-dimensional diffusion tensor microscopy of fixed mouse hearts. Magn. Reson. Med. 2004; 52:453–460. [PubMed: 15334561]

5. Scollan DF, Holmes A, Winslow R, Forder J. Histological validation of myocardial microstructure obtained from diffusion tensor magnetic resonance imaging. Am. J. Physiol. 1998; 275:H2308–H2318. [PubMed: 9843833]

6. Hsu EW, Muzikant AL, Matulevicius SA, Penland RC, Henriquez CS. Magnetic resonance myocardial fiber-orientation mapping with direct histological correlation. Am. J. Physiol. 1998; 274:H1627–H1634. [PubMed: 9612373]

7. Geerts L, Bovendeerd P, Nicolay K, Arts T. Characterization of the normal cardiac myofiber field in goat measured with MR-diffusion tensor imaging. Am. J. Physiol. Heart Circ. Physiol. 2002; 283:139–145.

8. Helm P, Beg MF, Miller MI, Winslow RL. Measuring and mapping cardiac fiber and laminar architecture using diffusion tensor MR imaging. Ann. NY Acad. Sci. 2005; 1047:296–307. [PubMed: 16093505]

9. Helm PA, Tseng HJ, Younes L, McVeigh ER, Winslow RL. Ex vivo 3D diffusion tensor imaging and quantification of cardiac laminar structure. Magn. Reson. Med. 2005; 54:850–859. [PubMed: 16149057]

10. Strijkers GJ, Bouts A, Blankesteijn WM, Peeters THJM, Vilanova A, van Prooijen MC, Sanders HMHF, Heijman E, Nicolay K. Diffusion tensor imaging of left ventricular remodeling in response to myocardial infarction in the mouse. NMR Biomed. 2009; 22:182–190. [PubMed: 18780284]

11. Chen J, Song SK, Liu W, McLean M, Allen JS, Tan J, Wickline SA, Yu X. Remodeling of cardiac fiber structure after infarction in rats quantified with diffusion tensor MRI. Am. J. Physiol. Heart Circ. Physiol. 2003; 285:H946–H954. [PubMed: 12763752]

12. Hsu EW, Xue R, Holmes A, Forder JR. Delayed reduction of tissue water diffusion after myocardial ischemia. Am. J. Physiol. 1998; 275:H697–H702. [PubMed: 9683460]

13. Plank G, Burton RAB, Hales P, Bishop M, Mansoori T, Bernabeu MO, Garny A, Prassl AJ, Bollensdorff C, Mason F, Mahmood F, Rodriguez B, Grau V, Schneider JE, Gavaghan D, Kohl P. Generation of histo-anatomically representative models of the individual heart: tools and application. Philos. Trans. Ser. A, Math. Phys. Eng. Sci. 2009; 367:2257–2292. [PubMed: 19414455]

14. Edelman RR, Gaa J, Wedeen VJ, Loh E, Hare JM, Prasad P, Li W. In vivo measurement of water diffusion in the human heart. Magn. Reson. Med. 1994; 32:423–428. [PubMed: 7984077]

15. Helander KG. Kinetic studies of formaldehyde binding in tissue. Biotech. Histochem. 1994; 69:177–179. [PubMed: 8068812]

16. Kiernan J. Formaldehyde, formalin, paraformaldehyde and glutaraldehyde: what they are and what they do. Microsc. Today. 2000; 8:8–12.

17. Paljärvi L, Garcia J, Kalimo H. The efficiency of aldehyde fixation for electron microscopy: stabilization of rat brain tissue to withstand osmotic stress. Histochem. J. 1979; 11:267–276. [PubMed: 110731]

18. Hopwood D. Some aspects of fixation with glutaraldehyde. A biochemical and histochemical comparison of the effects of formaldehyde and glutaraldehyde fixation on various enzymes and glycogen, with a note on penetration of glutaraldehyde into liver. J. Anat. 1967; 101:83–92. [PubMed: 6047703]

19. Karnovsky M. A formaldehyde–glutaraldehyde fixative of high osmolarity for use in electron microscopy. J. Cell Biol. 1965; 27:137A–138A.

20. Schmid P, Jaermann T, Boesiger P, Niederer PF, Lunkenheimer PP, Cryer CW, Anderson RH. Ventricular myocardial architecture as visualised in postmortem swine hearts using magnetic resonance diffusion tensor imaging. Eur. J. Cardiothorac. Surg. 2005; 27:468–472. [PubMed: 15740957]

21. Roebroeck A, Galuske R, Formisano E, Chiry O, Bratzke H, Ronen I, Kim DS, Goebel R. High-resolution diffusion tensor imaging and tractography of the human optic chiasm at 9.4 T. Neuroimage. 2008; 39:157–168. [PubMed: 17936015]

22. Schmitt B, Fedarava K, Falkenberg J, Rothaus K, Bodhey NK, Reischauer C, Kozerke S, Schnackenburg B, Westermann D, Lunkenheimer PP, Anderson RH, Berger F, Kuehne T. Three-dimensional alignment of the aggregated myocytes in the normal and hypertrophic murine heart. J. Appl. Physiol. 2009; 107:921–927. [PubMed: 19628727]

23. Rohmer D, Sitek A, Gullberg GT. Reconstruction and visualization of fiber and laminar structure in the normal human heart from ex vivo diffusion tensor magnetic resonance imaging (DTMRI) data. Invest. Radiol. 2007; 42:777–789. [PubMed: 18030201]

24. Shepherd TM, Thelwall PE, Stanisz GJ, Blackband SJ. Aldehyde fixative solutions alter the water relaxation and diffusion properties of nervous tissue. Magn. Reson. Med. 2009; 62:26–34. [PubMed: 19353660]

25. Yong-Hing CJ, Obenaus A, Stryker R, Tong K, Sarty GE. Magnetic resonance imaging and mathematical modeling of progressive formalin fixation of the human brain. Magn. Reson. Med. 2005; 54:324–332. [PubMed: 16032673]

26. Schmierer K, Wheeler-Kingshott CA, Tozer DJ, Boulby PA, Parkes HG, Yousry TA, Scaravilli F, Barker GJ, Tofts PS, Miller DH. Quantitative magnetic resonance of postmortem multiple sclerosis brain before and after fixation. Magn. Reson. Med. 2008; 59:268–277. [PubMed: 18228601]

27. Sun SW, Neil JJ, Song SK. Relative indices of water diffusion anisotropy are equivalent in live and formalin-fixed mouse brains. Magn. Reson. Med. 2003; 50:743–748. [PubMed: 14523960]

28. Shepherd TM, Flint JJ, Thelwall PE, Stanisz GJ, Mareci TH, Yachnis AT, Blackband SJ. Postmortem interval alters the water relaxation and diffusion properties of rat nervous tissue – implications for MRI studies of human autopsy samples. Neuroimage. 2009; 44:820–826. [PubMed: 18996206]

29. Kim TH, Zollinger L, Shi XF, Rose J, Jeong EK. Diffusion tensor imaging of ex vivo cervical spinal cord specimens: the immediate and long-term effects of fixation on diffusivity. Anat. Rec. (Hoboken). 2009; 292:234–241. [PubMed: 19051255]

30. Fishbein KW, Gluzband YA, Kaku M, Ambia-Sobhan H, Shapses SA, Yamauchi M, Spencer RG. Effects of formalin fixation and collagen cross-linking on T2 and magnetization transfer in bovine nasal cartilage. Magn. Reson. Med. 2007; 57:1000–1011. [PubMed: 17534923]

31. Thelwall PE, Shepherd TM, Stanisz GJ, Blackband SJ. Effects of temperature and aldehyde fixation on tissue water diffusion properties, studied in an erythrocyte ghost tissue model. Magn. Reson. Med. 2006; 56:282–289. [PubMed: 16841346]

32. Burton RAB, Plank G, Schneider JE, Grau V, Ahammer H, Keeling SL, Lee J, Smith NP, Gavaghan D, Trayanova N, Kohl P. Three-dimensional models of individual cardiac histoanatomy: tools and challenges. Ann. NY Acad. Sci. 2006; 1080:301–319. [PubMed: 17132791]

33. Deichmann R, Haase A. Quantification of T1 values by SNAPSHOT-FLASH NMR imaging. J. Magn. Reson. 1992; 96:608–612.

34. Jones DK, Horsfield MA, Simmons A. Optimal strategies for measuring diffusion in anisotropic systems by magnetic resonance imaging. Magn. Reson. Med. 1999; 42:515–525. [PubMed: 10467296]

35. Kingsley P. Introduction to diffusion tensor imaging mathematics: Parts I to III. Concepts Magn. Reson. Part A. 2006; 28A:101–122.

36. Streeter DD, Spotnitz HM, Patel DP, Ross J, Sonnenblick EH. Fiber orientation in the canine left ventricle during diastole and systole. Circ. Res. 1969; 24:339–347. [PubMed: 5766515]

37. Chen J, Liu W, Zhang H, Lacy L, Yang X, Song SK, Wickline SA, Yu X. Regional ventricular wall thickening reflects changes in cardiac fiber and sheet structure during contraction: quantification with diffusion tensor MRI. Am. J. Physiol. Heart Circ. Physiol. 2005; 289:H1898–H1907. [PubMed: 16219812]

38. Wu, Y.; Wu, EX. MR investigation of the coupling between myocardial fiber architecture and cardiac contraction. Conference Proceedings: Annual International Conference of the IEEE Engineering in Medicine and Biology Society; Minneapolis, Minnesota, USA. 2009; p. 4395-4398.

39. Pajevic S, Basser PJ. Parametric and non-parametric statistical analysis of DT-MRI data. J. Magn. Reson. 2003; 161:1–14. [PubMed: 12660106]

40. Jones DK. Determining and visualizing uncertainty in estimates of fiber orientation from diffusion tensor MRI. Magn. Reson. Med. 2003; 49:7–12. [PubMed: 12509814]

41. Bossart, E.; Inglis, B.; Silver, X.; Mareci, TH. The effect of fixative solutions in magnetic resonance imaging. Proceedings of the 7th Annual Meeting of ISMRM; Philadelphia, PA, USA. 1999; p. 1928

42. Kobayashi M, Kawamura K, Honma M, Masuda H, Suzuki Y, Hasegawa H. Tunnel capillaries of cardiac myocyte in pressure-overloaded rat heart – an ultrastructural three-dimensional study. Microvasc. Res. 1999; 57:258–272. [PubMed: 10329252]

43. Bishop MJ, Plank G, Burton RAB, Schneider JE, Gavaghan DJ, Grau V, Kohl P. Development of an anatomically detailed MRI-derived rabbit ventricular model and assessment of its impact on simulations of electrophysiological function. Am. J. Physiol. Heart Circ. Physiol. 2010; 298:H699–H718. [PubMed: 19933417]
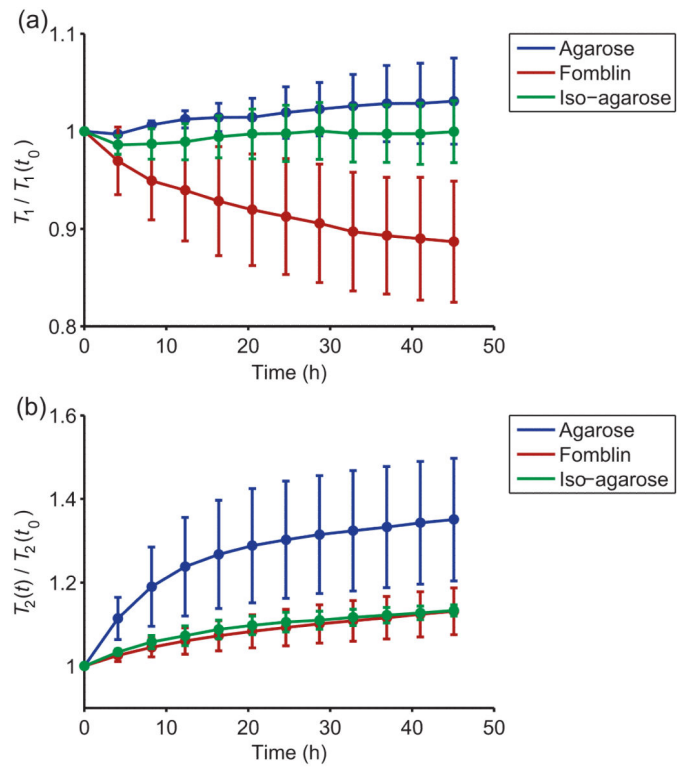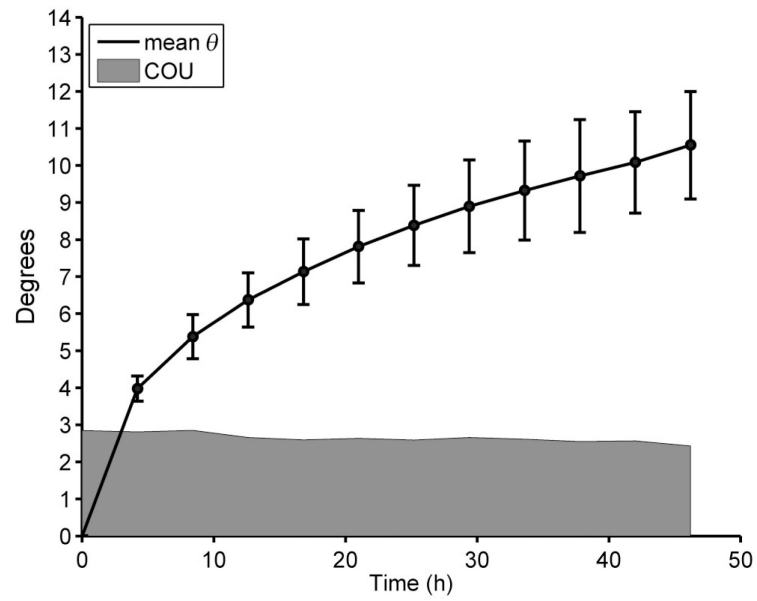
Figure 1.
Temporal evolution of mean myocardial T_1 (a) and T_2 (b) values for all heart preparations. Within each group, data points are normalised to the value measured at the first time point (t_0). Data points represent means for each group; error bars are standard deviations.
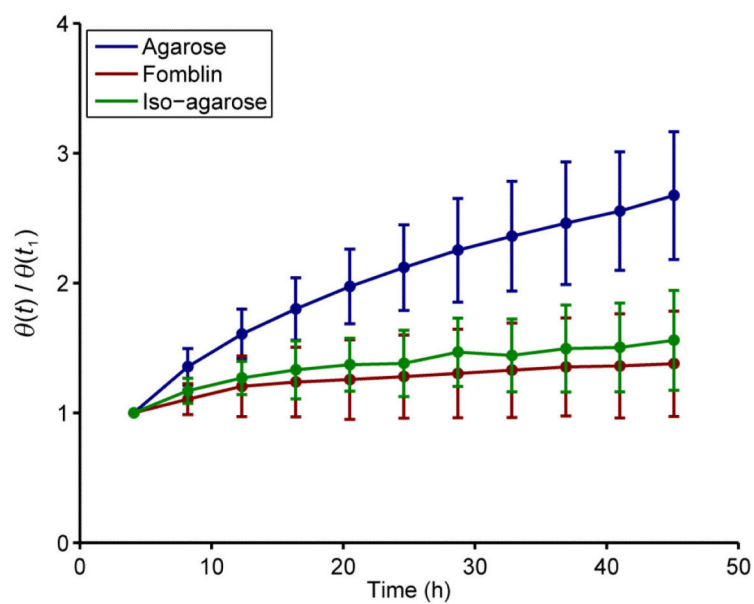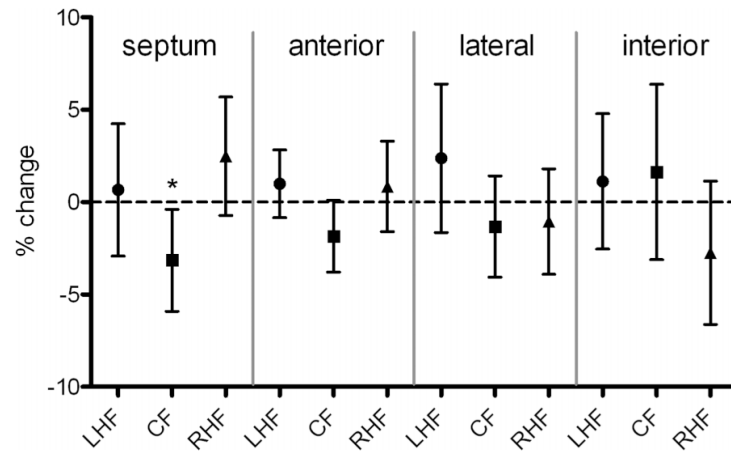
Figure 2.
Time series plot of θ, the mean angular deviation of the primary eigenvector from its original value at t_0, for each preparation. Within each group, values of θ are normalised to the value at t_1. Data points represent the mean $\pm$ standard deviation for each group.

Figure 3.
Measured vales of θ as a function of time for the standard agarose-embedded hearts (i). The shaded area shows the cone of uncertainty (COU) around the orientation of v_1, based on the bootstrap analysis of the diffusion tensor imaging (DTI) data. Data points represent the mean of the three hearts in this group; error bars are standard deviations.

Figure 4.
Mean change in percentage of left-handed helical fibres (LHF), circumferential fibres (CF) and right-handed helical fibres (RHF) at t_f in the four walls of the left ventricle. Data points show the mean values for all hearts; error bars show 95% confidence intervals. *Statistically significant change ($p < 0.05$).

Table 1

Fixative and buffer used in this investigation. All solutions at controlled pH (pH 7.4)

Solution	Paraformaldehyde	Sodium cacodylate	Glutaraldehyde (50%)	Osmolarity (mOsm)
Karnovsky (200 mL)	4 g in 100 mL H_2O, pH 7.4	4.28 g in 100 mL H_2O, pH 7.4	8 mL in 100 mL H_2O	1210 ± 5
Cacodylate buffer		4.28 g in 100 mL H_2O, pH 7.4		385 ± 5

Table 2

Values for T_1, T_2, fractional anisotropy (FA) and apparent diffusion coefficient (ADC) in the myocardium at t_0 (mean ± standard deviation)

Preparation	T_1 (ms)	T_2 (ms)	FA	ADC ($\times 10^{-4}$, mm^2/s)
(i) Standard agarose	879 ± 63[iii]	41.8 ± 8.2	0.28 ± 0.03	8.81 ± 0.13
(ii) Fomblin	787 ± 62[iii]	27.5 ± 1.5[iii]	0.27 ± 0.02	7.99 ± 0.60
(iii) Iso-osmotic agarose	1247 ± 124[i,ii]	53 ± 16[ii]	0.25 ± 0.03	8.74 ± 0.77

All values are means ± standard deviation. Mean value of T_1 in (iii) is statistically significantly different from that in (i) ($p < 0.01$) and (ii) ($p < 0.001$). There is no statistically significant difference between T_1 in (i) and (ii) ($p > 0.05$). The only significant difference in T_2 values is between groups (ii) and (iii) ($p < 0.05$). There are no statistically significant differences between the mean FA and ADC values from each group. All comparisons determined by one-way analysis of variance followed by *post-hoc* Bonferroni multiple comparisons with other preparations. Superscripts show which preparations are significantly different within each category.

Table 3

Change in value of the cone of uncertainty (δCOU), θ ($\delta\theta$) and signal-to-noise ratio (δSNR) at t_f for each preparation

Preparation	δCOU (deg) at t_f	$\delta\theta$ (deg) at t_f	δSNR (%) at t_f
(i) Standard agarose	0.3	6.6	11.7 ± 9.4
(ii) Fomblin	0.4	3.2	8.9 ± 5.8
(iii) Iso-osmotic agarose	0.3	1.9	12.0 ± 6.7